STUDY OF PLL LESS DSGTP SYSTEM USING BAND-PASS FILTER AND APC (ACTIVE POWER COEFFICIENT) CONTROL

Saptaparna Basu Roy Chowdhury[1*] – Atanu Maji[1] – Sk Rabiul Hossain[1] - Pritam Kumar Gayen[2]

[1] Department of Electrical Engineering, Cooch Behar Government Engineering College, PIN-736170, West Bengal, India
[2] Department of Electrical Engineering, Kalyani Government Engineering College, PIN-741235, West Bengal, India

ARTICLE INFO

***Article history*:**
Received: 14.03.2024.
Received in revised form: 23.04.2024.
Accepted: 25.07.2024.

Keywords:
Double stage grid tied photovoltaic (DSGTP) system
Active Power Coefficient (APC) control
Phase locked loop (PLL)
Band-pass filter
Total harmonic distortion (THD)

DOI: https://doi.org/10.30765/er.2470

Abstract:

This paper represents a study on a grid-tied photovoltaic (PV) system connected to a non-linear load. The system includes a PV array, a boost converter, a voltage source inverter (VSI), and a coupling inductor for grid connection. The maximum power point tracking (MPPT) mechanism based on Perturb and Observe (P&O) method which is used to control the duty ratio of the boost converter. Synchronization is achieved through a second-order band-pass filter instead of a Phase Locked Loop (PLL). However, the non-linear load causes poor current quality, leading to a high Total Harmonic Distortion (THD) in the grid current, which may affect the sinusoidal nature of the grid current and other connected loads. To address the harmonics problem, an Active Power Coefficient (APC) control technique is implemented to control the PV inverter gate pulse. The proposed model has been simulated in Matlab/Simulink, and system output parameters are analysed graphically. The simulation results indicate that the proposed approach maintains the total harmonic distortion (THD) of the grid current below 5% even in changing weather conditions, which satisfies the IEEE 519 standard.

1 Introduction

The increasing demand for energy, the concerning pace of global warming, and the exhaustion of natural resources are forcing humanity to opt for alternative and clean energy sources to minimize carbon emissions and maintain the sustainability of our planet and its surroundings. Photovoltaic (PV) sources offer a promising solution to these issues. However, there are several obstacles that need to be addressed to ensure a successful integration of PV sources into the grid system. The solar systems have some drawbacks such as the nonlinear current (I) vs. voltage (V) and power (P) vs. voltage (V) characteristics. Additionally, the maximum power point (MPP) tends to vary due to fluctuating weather conditions. Previous studies [1-7] have addressed this issue. Typically, single-stage (DC-AC) and double-stage (DC-DC & then DC-AC) methods are used to connect isolated solar PV systems with the power grid system [8]. However, in current circumstances, a large number of power electronic converters are required, which degrades the power quality (PQ) of the grid. Moreover, the intermittent nature of solar irradiance affects the quality and continuity of the overall system, making it necessary to deploy advanced control methods and prefer the single-stage topology to ensure reliable and continuous active power supply to the grid from the connected solar PV system.

This approach is crucial for maintaining and monitoring power quality conditioning [9]. Many researchers have proposed several ways for the improvement of power quality of the grid connected PV system, out of which a large number of researches aim at time and frequency domain analysis based control algorithms, especially for the operation of grid-connected voltage source converter (VSC). But in most of the cases, frequency analysis based topologies are computationally heavier and hence, requires high-memory and high-speed digital controllers and complicated algorithms for accurate implementation. Thus the computational

* Corresponding author
E-mail address: saptabasu6@gmail.com

burden on the system becomes higher along with the cost of controller. Besides, these analyses further require larger sampling time for effective harmonic decomposition [10]; hence becomes harder to implement. Thus, time domain controls are mostly used for grid connected solar PV applications and hardware implementation is done through the real-time controllers. In this study, the Perturb & Observe (P&O) algorithm was utilized to identify the maximum power point. While stand-alone PV cells have various applications, grid-connected PV systems have their own set of benefits and uses. These systems offer enhanced energy security by reducing dependence on non-renewable resources and shifting towards greener energy. Many synchronization techniques for grid-connected systems have been examined by researchers [11-15]. In this work, voltage source inverters (VSI) were preferred over current source inverters (CSI) due to the latter's problematic dynamic characteristics [16]. Controlling the DC link voltage is a crucial aspect of the system, as sudden disturbances may significantly alter capacitor voltage and negatively impact the overall performance. To stabilize the DC link voltage, a PI controller was used, which is known for its ability to minimize steady-state errors. Several studies have implemented PI controllers for similar applications [17-21]. In most of these studies, power quality was assessed using the total harmonic distortion (THD) parameter, which measures undesirable harmonic components in a signal. During unbalanced conditions or sudden disturbances, higher-order frequency harmonics can undesirably distort the signal. Hence, THD analysis is essential for evaluating power quality [22]. As per IEEE 519-2014 [23], permissible THD for bus voltage at the point of common coupling $V \leq 1$ kV should be under 8%. In this experiment, THD was calculated for load, grid, and inverter current using Fast Fourier Transform (FFT) and analysed graphically. In the present work, grid voltage is converted from line to phase quantity followed by alpha-beta quadrature form using Clarke transformation.

This is followed by the unit vector voltage generation using band-pass filter. Next the load current has been calculated using the active Power Coefficient (APC) method and using the unit vectors so produced. This is followed by inverter gate pulse generation. DC link voltage control is achieved by using suitable PI controller. The major advantage of the system is that the proposed model serves good to deliver active power to the load as well as transfer the excess active power to the grid, without absorbing any reactive power from the grid; thereby, retaining a good quality of power with less than 2% harmonic distortion (THD); which is, as per the IEEE standard 519-2014 [23], very much acceptable under all circumstances. Although, similar works have been practices by researchers [24], but the more important feature of the proposed work lies in the fact that this output is achieved without using phase locked loop (PLL) in the present study. The study described in reference [25] evaluates how well a double-stage grid-connected photovoltaic (DSGCP) system functions with a non-linear load during regular operation and when faced with different types of grid faults. This evaluation is carried out using a control strategy based on a phase-locked loop (PLL). In this study, a prototype PV model was created using Matlab-Simulink, and various system parameters were observed. Voltage, reactive and active power profiles of the inverter, load, and grid were examined, along with the change of capacitor voltage over time. Furthermore, the harmonics of inverter current, load current, and grid current waveforms were analysed. Result-oriented discussions were carried out based on the necessary findings.

2 Methods

In the field of renewable energy, there has been a growing interest in incorporating photovoltaic (PV) systems into the existing electric grid, which can be attributed to the rising demand for sustainable energy sources. However, the integration of PV systems also brings challenges, such as harmonic distortion, which can affect the quality of the electric power supplied to the grid. In order to mitigate these harmonic distortions, various control strategies have been proposed, including the use of Active Power Coefficient (APC) control. The aim of this chapter is to represent a study on the harmonic mitigation of double-stage grid-tied photovoltaic systems using APC control. The chapter will provide a comprehensive overview of the APC control strategy, including its design and implementation, as well as the results and discussion of the study. The outcomes of this work will contribute to a deeper understanding of the potential of APC control in improving the integration of PV systems into the electric grid, while ensuring the quality of the electric power supplied to the grid.

2.1 Objectives of the proposed work

The objectives of the proposed work are as follows:

• The first objective of the present study is to model an APC controlled DSGTP system without using the PLL technology i.e., designing a PLL less APC controlled DSGTP system.

• Different case studies have been investigated thereafter depending upon diverse weather conditions. Solar cells are often dependant on the weather conditions since the intensity of irradiation depends on how much overcast the sky is, or the direction of the sun and the clouds etc.

• Another major objective of the work is to study the nature of harmonics and power flow dynamics; since the balance between the ratios of reactive to active power consumed by the load and that of the generation often causes harmonics in the system, and hence, further promotes imbalance to the power factor of the circuit.

• The algorithm proposed in this study aims to address harmonic disturbances by balancing the reactive power demand of the system. To achieve this, the algorithm ensures that the active power demand of the load is met by both the power generated by the PV system and the grid. However, the reactive power demand is solely managed by the PV inverter and not the grid. This approach ensures that the grid power factor is not compromised. Even when there is no irradiation, the installed solar inverter is capable of supplying the net reactive power demand of the load. Essentially, the proposed design functions as a power factor compensatory device similar to a STATCOM.

• Finally, a comparative study has been proposed in order to compare the proposed method with other contemporary schemes with similar objectives.

In order to design the proposed scheme, we have adopted a double stage PV inverter design scheme in this case. Perturb & Observe method has been implemented here to locate the maximum power point (MPP) in the system in the initial phase. The main benefit of the proposed scheme is that it has been designed without implementing phase locked loop (PLL), which is a common scheme in several models [24]. Further we have incorporated band-pass filter in the design. The design is further based on the unit voltage vector concept, i.e., the voltages have been converted to per unit model for generalization of design; as well as used active power coefficient (APC) control for final implementation of the scheme.

2.2 Perturb & Observe method

This method is implemented in the present scheme in order to perform the maximum power point tracking (MPPT). When a PV system is operating at point outside (to the left) maximum power point (MPP), the magnitudes of voltage, current and Power are measured initially. Next the terminal voltage is increased slightly and the operating point moves slightly towards right side. This is the new operating point for the PV system where the voltage, current and power is measured again. Now if power measured at this new point (to the right side) is greater than previously measured point (to the left side), the terminal voltage is further increased and the voltage, current and power is measured again at this new point. These new parameters are again compared to the immediately recorded previous set of values and the same process is repeated till the MPP is reached. This is ensured as when the MPP is reached, a slight increase the terminal voltage results in slightly reduced power at new point compared to MPP. In that case, the terminal voltage is again decreased to shift back to MPP again.

Thus, this process of tracking the MPP is primarily an iterative scheme. But the major drawback with this method is that the operating point oscillates about the MPP in an equilibrium state and is never settled. The band of oscillation, however, may be reduced by decreasing the rate of voltage increment in each step. This is one of the easiest ways to overcome this problem, with a compromise to the speed of operation for searching towards the MPP, as well as slowing down of the overall system. Another major disadvantage of this method is experienced during the fast changing atmospheric conditions. Perturb & Observe method shifts the operating point away from the MPP until stable atmospheric condition is arrived during the fast changing weathers. This results in a good amount of power loss and hence the system efficiency is further reduced. In our application, the Perturb and Observe (P&O) method has demonstrated satisfactory performance and has met our requirements, attributable to its straightforward algorithms and logical design.

2.3 Control algorithm

The entire control scheme of the proposed work is divided in the following segments as follows:

• The classical perturb and observe (P&O) MPPT technique is used for maximum power point tracking (MPPT), where the DC-link reference voltage is determined based on the maximum extracted power.

• Voltage control and harmonic mitigation have been achieved using the proposed active power coefficient (APC) control.

• The proportional integral (PI) controller works towards maintaining the DC link voltage at the desired reference voltage point.

• In addition, we have implemented synchronization in our system without the use of a Phase Locked Loop (PLL). Rather, we have employed a second order band-pass filter, which not only simplifies our system but also reduces its complexity.

• To retain almost unity power factor of the grid to avoid any penalty. Hence, the proposed design works additionally similar to the reactive power compensatory device such as the STATCOM; although, allows for only active power intake during the shortfall of active power on the load side.

3 Designing of the proposed model

3.1 Overall system design

The schematic diagram of the Matlab simulated model of the proposed grid connected double stage PV scheme is shown in Figure 1. The detailed parameters of the PV array and that of the individual PV modules are also describe in Table 1 and Table 2 respectively.

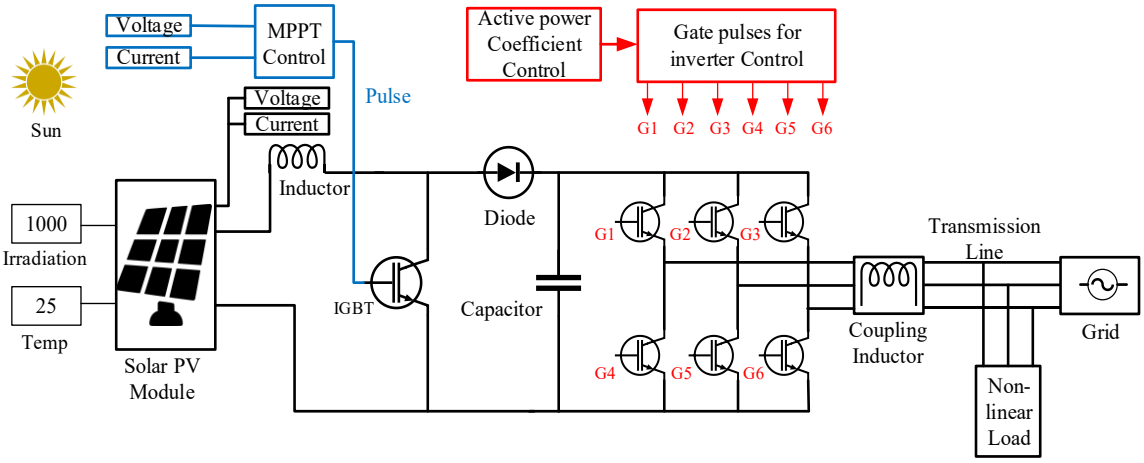

Figure 1. Schematic diagram of the proposed model.

Table 1. PV array specification.

Parameter	Value
Modules connected in parallel	12
Incident solar insolation (W/m2)	0, 400, 1000
Modules connected in series	7
Temperature (°C)	25

Table 2. One PV module specifications.

Parameter	Value
Crest Power (W)	315.07
Maximum power point voltage Vmp (V)	54.70
Open Circuit Voltage V_{OC} (V)	64.5
Maximum power point current Imp (A)	5.75

Some of the other major parameters of the simulated system are described below:

- DC link Capacitor ratting = 3000 micro Farad
- Coupling inductor ratting = 2.5 mH
- Details of the non-linear type of R-L load:
  Resistance = 25 Ohm
  Inductance =50mH
  Active power drawn = 9000 Watt (approx.),
  Reactive power drawn = 5000 VAR (approx.)
- Grid parameters:
  Voltage = 415 Volts (line to line RMS),
  Frequency = 50 Hz.

3.2 Grid voltage conversion

The grid voltage conversion has been done in the following way as described in Figure 2.

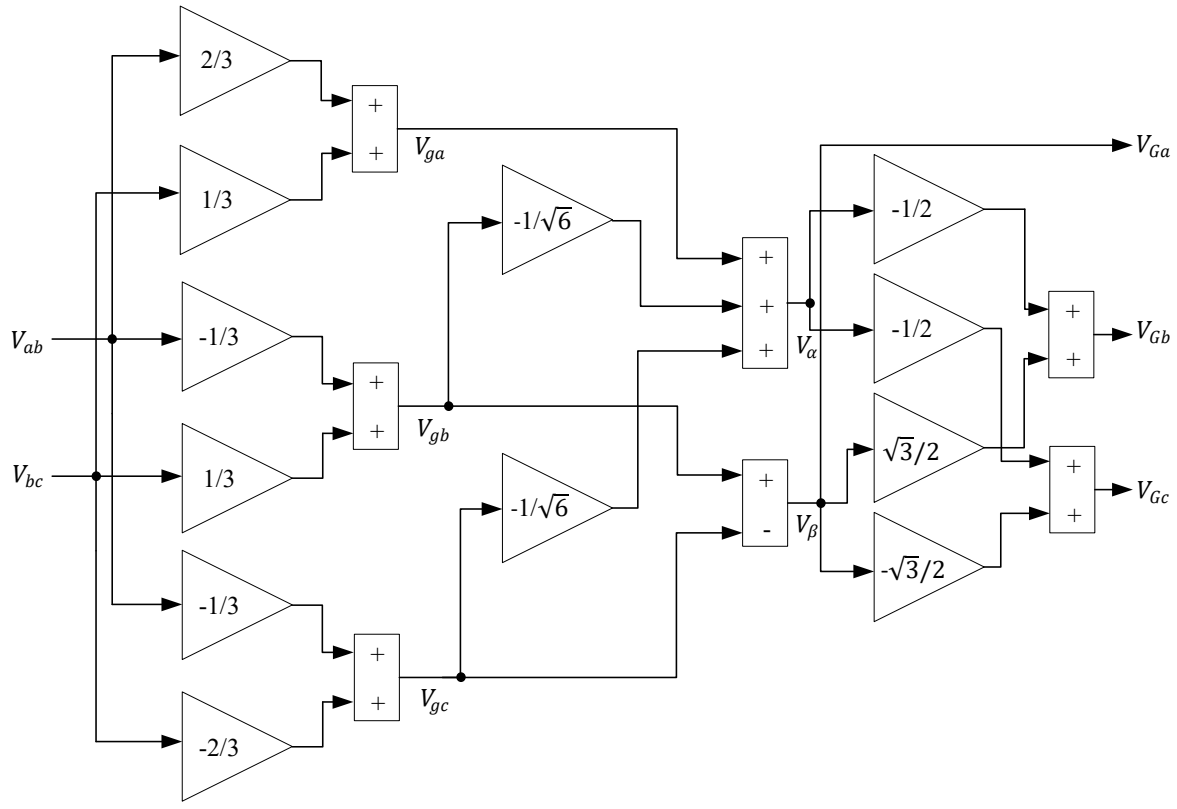

Figure 2. Schematic diagram for grid voltage conversion.

As described in Figure 2, the grid line voltage is initially converted to grid phase voltage as per the expression given by equation (1). The line A to line B voltage (V_{ab}) and the line B to line C voltage (V_{bc}) are multiplied with the conversion matrix to yield the three phase voltages V_{ga}, V_{gb} and V_{gc} respectively as follows:

$$\begin{bmatrix} V_{ga} \\ V_{gb} \\ V_{gc} \end{bmatrix} = \begin{bmatrix} 2/3 & 1/3 \\ -1/3 & 1/3 \\ -1/3 & -2/3 \end{bmatrix} \times \begin{bmatrix} V_{ab} \\ V_{bc} \end{bmatrix} \tag{1}$$

The grid phase voltages are next converted to alpha-beta form using Clarke transformation as per the equation (2) as follows:

$$\begin{bmatrix} V_{\alpha} \\ V_{\beta} \end{bmatrix} = \sqrt{\frac{2}{3}} \times \begin{bmatrix} 1 & -1/2 & -1/2 \\ 0 & \sqrt{3}/2 & -\sqrt{3}/2 \end{bmatrix} \times \begin{bmatrix} V_{ga} \\ V_{gb} \\ V_{gc} \end{bmatrix} \tag{2}$$

These quadrature voltages in the form of alpha-beta voltages are next converted to grid phase voltages for the three phases using inverse Clarke transform as follows:

$$\begin{bmatrix} V_{Ga} \\ V_{Gb} \\ V_{Gc} \end{bmatrix} = \begin{bmatrix} 1 & 0 \\ -1/2 & \sqrt{3}/2 \\ -1/2 & -\sqrt{3}/2 \end{bmatrix} \times \begin{bmatrix} V_{\alpha} \\ V_{\beta} \end{bmatrix} \tag{3}$$

3.3 Unit vector voltage generation using band-pass filter

These three phase converted grid voltages are passed through suitable band-pass filter to obtain the three phase filtered voltages in as per the schematic simulation diagram shown in Figure 3.

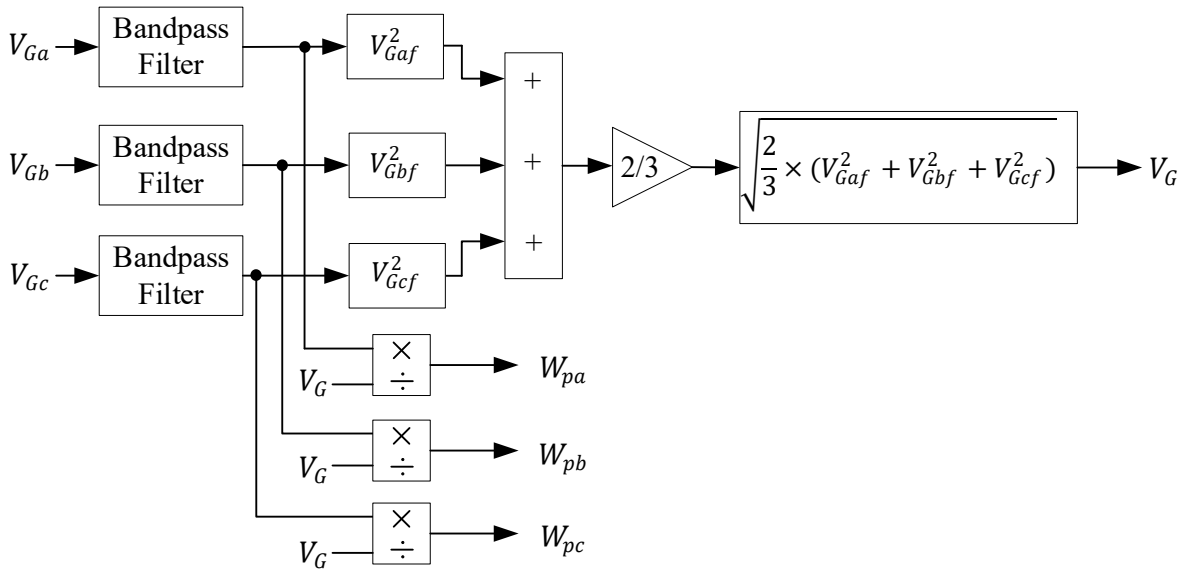

Figure 3. Schematic diagram for terminal grid voltage and unit vector voltage generation.

The chosen transfer function of the digital band pass filter is considered as $H_{BP}(z)$as follows:

$$H_{BP}(z) = \frac{k * (1 - z^{-1})}{\left[1 - (k-2)z^{-1} + \left(1 - k + \frac{k^2}{2}\right)z^{-2}\right]} \tag{4}$$

Where the parameter *k* is taken as $k = 44 \times 10^{-5}$
Each phase voltage of the corresponding grid is passed through this filter to obtain the filtered phase voltages V_{Gaf}, V_{Gbf} and V_{Gcf} respectively as per expressions (5) to (7) as follows:

$$V_{Ga} \xrightarrow{Band\ pass\ filter} V_{Gaf} \tag{5}$$

$$V_{Gb} \xrightarrow{Band\ pass\ filter} V_{Gbf} \tag{6}$$

$$V_{Gc} \xrightarrow{Band\ pass\ filter} V_{Gcf} \tag{7}$$

The terminal grid voltage (V_G) is further obtained by squaring each of these filtered phase voltage, scaling and finally taking the square root of the same as per equation (8) below:

$$V_G = \sqrt{\frac{2}{3} \times (V_{Gaf}^2 + V_{Gbf}^2 + V_{Gcf}^2)} \tag{8}$$

The unit vector voltages for each phase e.g., w_{pa}, w_{pb} and w_{pc} are obtained respectively by dividing each of the filtered phase voltages i.e., V_{Gaf}, V_{Gbf} and V_{Gcf} with the terminal grid voltage (V_G) as below:

$$w_{pa} = \frac{V_{Gaf}}{V_G} \tag{9}$$

$$w_{pb} = \frac{V_{Gbf}}{V_G} \tag{10}$$

$$w_{pc} = \frac{V_{Gcf}}{V_G} \tag{11}$$

3.4 Load current calculations (APC method)

The load currents are further computed using the APC method. This is done by taking the ratio of the integral of the product of each line current and the unit vector voltage of the corresponding phase i.e., $\int (I_{li} \times w_{pi})\, dt$ to the integral of the square of the unit vector voltage of the same phase $\int w_{pi}^2\, dt$; where, *i* denotes each of the three phases *a. b* and *c* respectively. These expressions are given by the following equations:

$$I_{lax} = \frac{\int \left(I_{la} \times w_{pa}\right) dt}{\int w_{pa}^2 \; dt} \tag{12}$$

$$I_{lbx} = \frac{\int \left(I_{lb} \times w_{pb}\right) dt}{\int w_{pb}^2 \; dt} \tag{13}$$

$$I_{lcx} = \frac{\int \left(I_{lc} \times w_{pc}\right) dt}{\int w_{pc}^2 \; dt} \tag{14}$$

Thus, the final average line current is computed by taking the mean of all the three phase modulated line currents as below:

$$I_{lavg} = \frac{I_{lax} + I_{lbx} + I_{lcx}}{3} \tag{15}$$

The entire scheme is described as shown in Figure 4 and the Matlab simulation diagram is described in Figure 5.

3.5 DC link Capacitor voltage control and gate pulse generation

The next task is to control the capacitor voltage and generation of the gate pulses. This scheme is represented using Figure 5 using schematic and Matlab simulink diagrams. This is done initially by computing the error component (ϵ_{dc}) between the DC link reference voltage and the measured capacitor voltage as per equation (16).

$$\epsilon_{dc} = \left(V_{dc}^{m} - V_{dc}^{ref}\right) \tag{16}$$

This DC link error component (ϵ_{dc}) is further passed through a proportional integral controller (PI controller) to obtain an equivalent DC current component I_d as follows:

$$\epsilon_{dc} \xrightarrow{PI\ Controller} I_d \tag{17}$$

The transfer function of the digital PI controller is considered as $H_{PI}(z)$ as follows:

$$H_{PI}(z) = P\left(1 + I * T_s \frac{1}{z-1}\right) \tag{18}$$

Where the control parameter is adjusted as Ts (simulation step time) = 0.0001 in simulation.

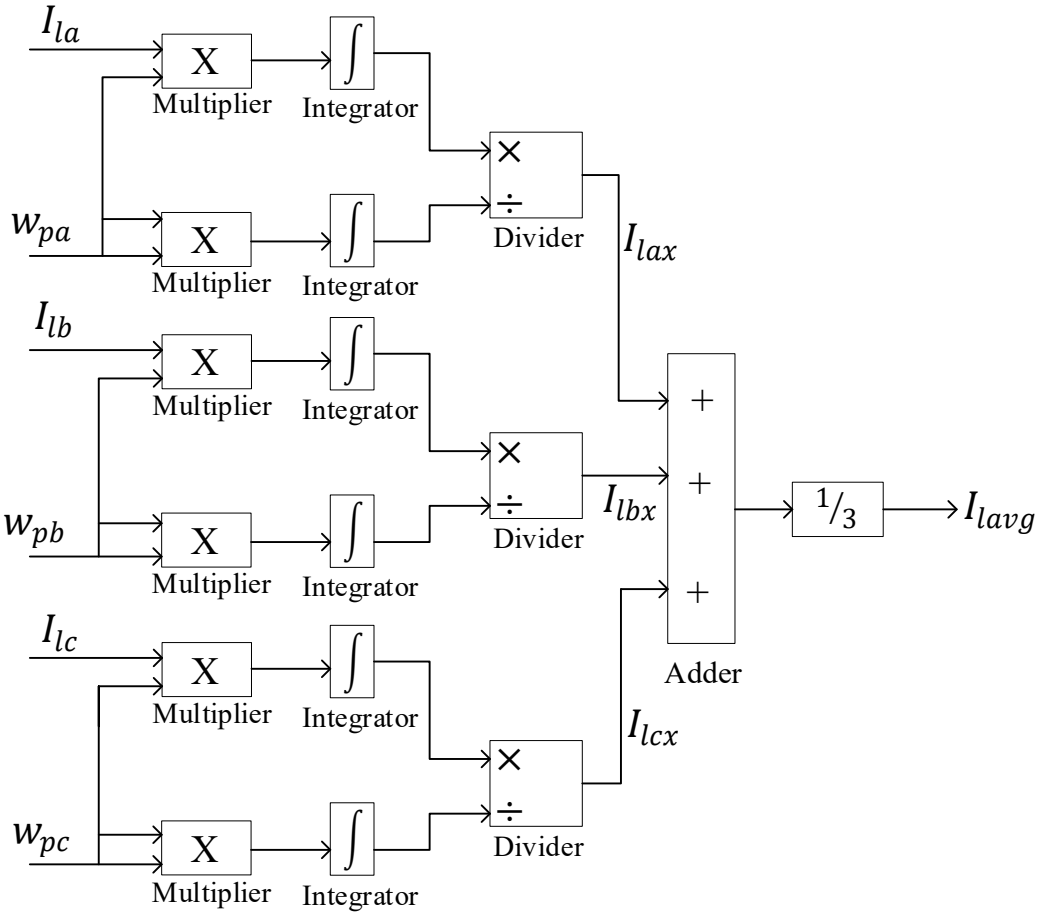

Figure 4. Schematic diagram for Load current calculations by APC method.

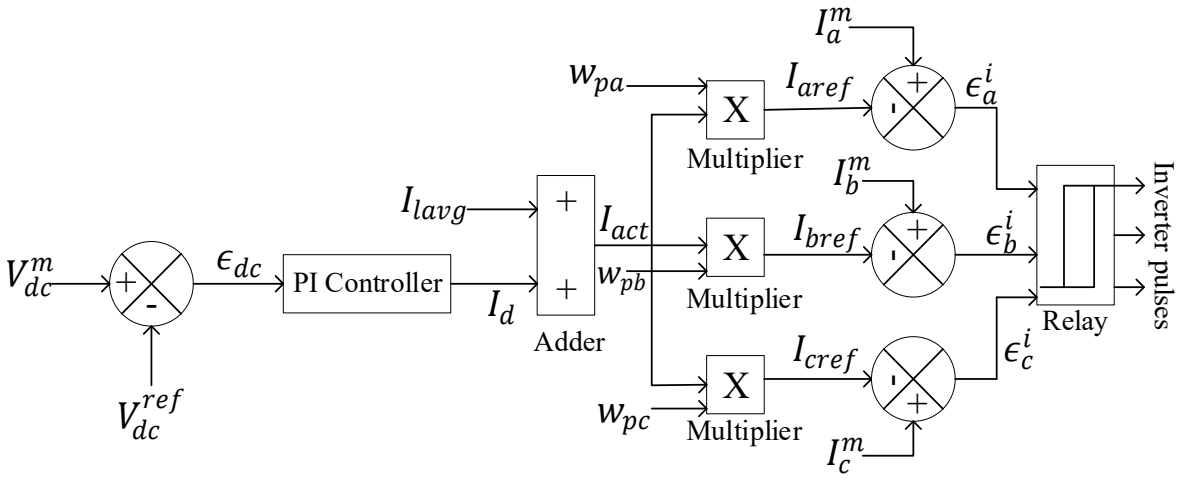

Figure 5. Schematic diagram for DC link voltage control and inverter gate pulse generation.

This controlled equivalent current component I_d so formed is added to the average line current developed in the previous stage I_{lavg} to obtain the actual line current I_{act} as follows:

$$I_{act} = I_{lavg} + I_d \tag{19}$$

The three phase reference currents i.e., I_{aref}, I_{bref} and I_{cref} respectively are further developed by multiplying this actual line current I_{act} so developed with the unit vector voltages for each phase e.g., w_{pa}, w_{pb} and w_{pc} as follows:

$$I_{aref} = I_{act} \times w_{pa} \tag{20}$$

$$I_{bref} = I_{act} \times w_{pb} \tag{21}$$

$$I_{cref} = I_{act} \times w_{pc} \tag{22}$$

The corresponding phase current errors are next developed by comparing each of these three phase reference currents i.e., I_{aref}, I_{bref} and I_{cref} with those of the measured line currents of the three phases i.e., I_a^m, I_b^m and I_c^m respectively. These errors are given as:

$$\epsilon_a^i = (I_a^m - I_{aref}) \tag{23}$$

$$\epsilon_b^i = (I_b^m - I_{bref}) \tag{24}$$

$$\epsilon_c^i = (I_c^m - I_{cref}) \tag{25}$$

ϵ_a^i, ϵ_b^i, ϵ_c^i are finally processed via hysteresis relay to develop gate pulses for the voltage source inverter (VSI) in the proposed scheme.

4 Result and Discussion

In the proposed work, the net irradiation on the PV cells has been adjusted in three stages as follows:

a) For t=0 to 0.4 sec, Irradiation = 0
b) For t=0.4 to 0.8 sec, Irradiation = 400 Watt/m^2
c) For t =0.8 to 1.2 sec, Irradiation = 1000 Watt/m^2

This variation of irradiance is shown graphically in Figure 6(a). As is mentioned here that we have varied the irradiation level in three steps, the objective of the work is to observe the reactive and active power delivered to the load by the PV cells under this varying irradiation level; also the voltage and current pattern and harmonic distortion under each level separately.

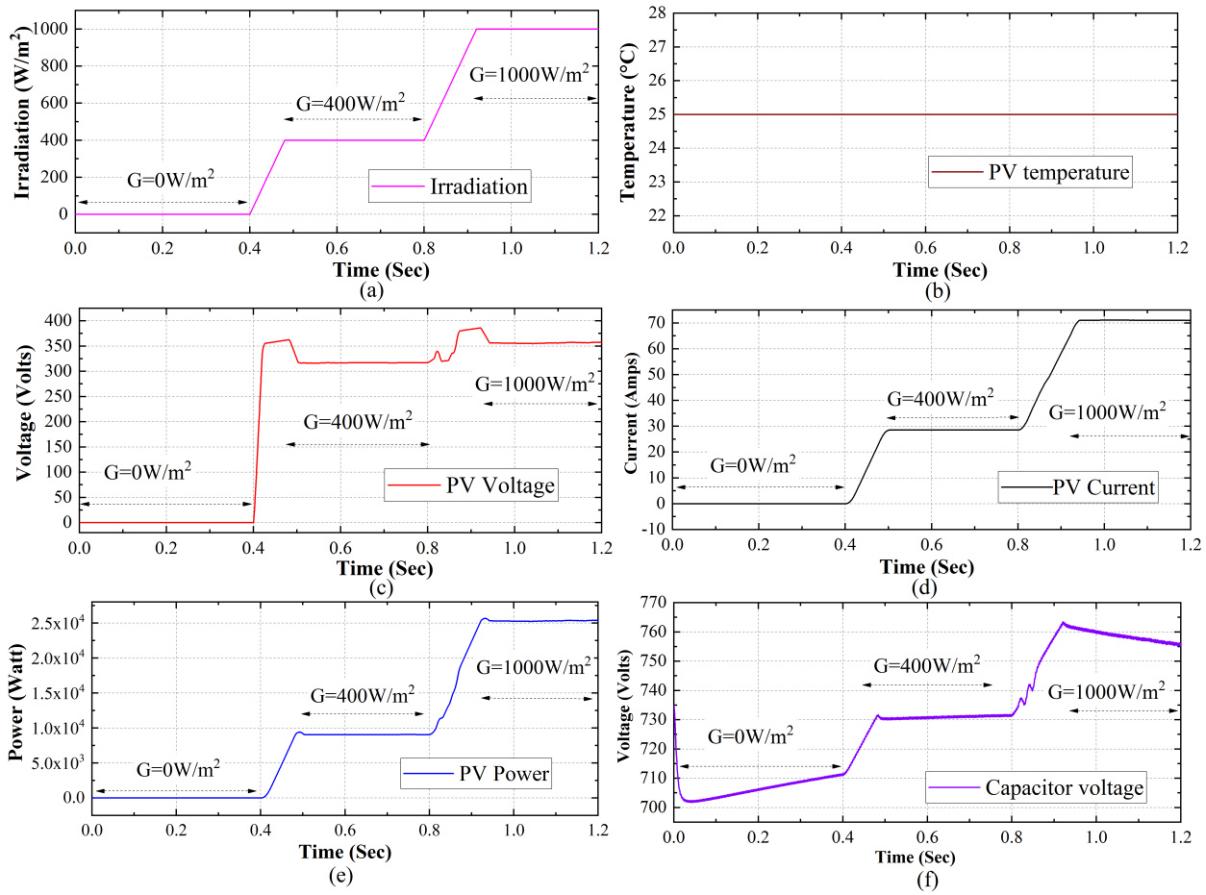

Figure 6. Waveforms representing the input output characteristics of the simulated model: (a) the variation of the irradiation level in three steps, (b) variation of temperature level of the PV module, (c) PV array output voltage profile, (d) PV array output current profile, (e) PV array output active power profile, (f) variation of the voltage across the DC link capacitor.

In order to observe the same, we have plotted the current, voltage and power profiles of the PV output and that of the connected grid. The input parameters to the cells are the varying irradiation level and we have also monitored the temperature pattern of the cells. Figure 6 (a) represent graphically how the irradiation level has varied with time. It is easily observed that this level of illumination remains zero for the first 0.4 sec, when we can consider almost absolutely dark condition, may be at night. Next we have varied the irradiation level at 400 W/m^2 for the next 0.4 sec to simulate overcast condition; and finally, we have set the irradiation level to 1000 W/m^2 in order to simulate completely sunny weather condition. The temperature level is shown in Figure 6(b) where the PV module temperature is set constant at 25 degree Celsius under all irradiation levels. Figure 6(c) to Figure 6(f) describes the output characteristics of the PV modules. Figure 6(c) displays the output voltage profile of the modules which describes that the module output voltage remains close to zero when the irradiation level is zero.

This is understandable as the output from the modules ceases in absence of any irradiation. Next when the irradiation level goes upto 400 W/m^2, the PV array voltage raises to nearly 300V DC, following minor transient disturbance. Further, when the radiation level research 1000 W/m^2, the voltage level increases slightly to nearly 350V, again followed by little transient disturbances. We have used P&O method to find out the maximum power point (MPP) in the proposed work; hence, the PV current and the PV active power profiles match the irradiation level in each of the steps, i.e., the power and the current profiles also increases in steps in synchronism to the variation of the three step irradiation level. The PV power shown here reflects the DC power produced by the PV modules. The voltage across the capacitor also follows similar pattern as shown in Figure 6(f).

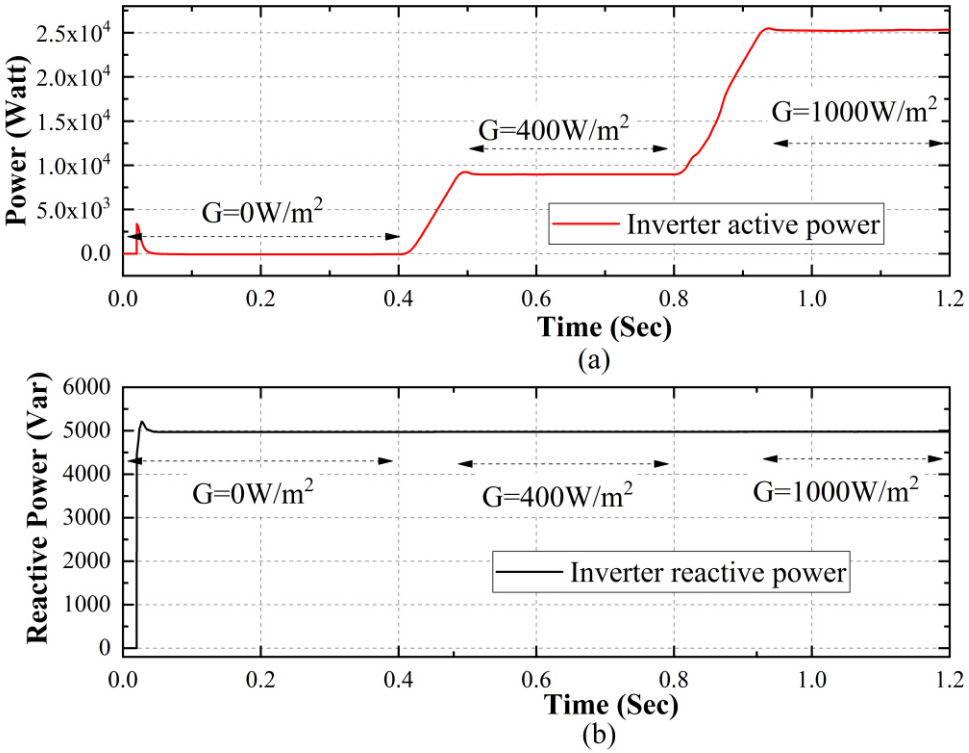

Figure 7. Power profiles of the PV inverter with variation in irradiation level: (a) inverter output active power profile, (b) inverter output reactive power profile.

The solar inverter active and reactive power profiles are described in Figure 7(a) and Figure 7(b) respectively. Figure 8 shows the similar characteristic of the grid. Figure 9(a) and Figure 9(b) displays respectively the active and reactive power demand of the load.

4.1 Analysis of active power distribution

It is observed that the load constantly requires and active power of about 9 kW as is shown in Figure 9(a). The inverter active power ranges in the level of 9 kW and 25 kW under the solar insolation levels of 400 W/m^2 and 1000 W/m^2 respectively as is observed from Figure 7(a). Thus, it is observed that the inverter produced active power is entirely consumed by the load under irradiation level of 400 W/m^2 and hence, the inverter neither receives any active power from the grid, nor it supplies any to the grid. Thus the grid active power level remains nearly zero as shown in Figure 8(a). Thus, the PV unit remains floating with respect to the grid under such circumstances in terms of active power delivery under 400 W/m^2 irradiation level. But the scenario reverses for the next level of irradiation of 1000 W/m^2 for the next 0.4 sec.

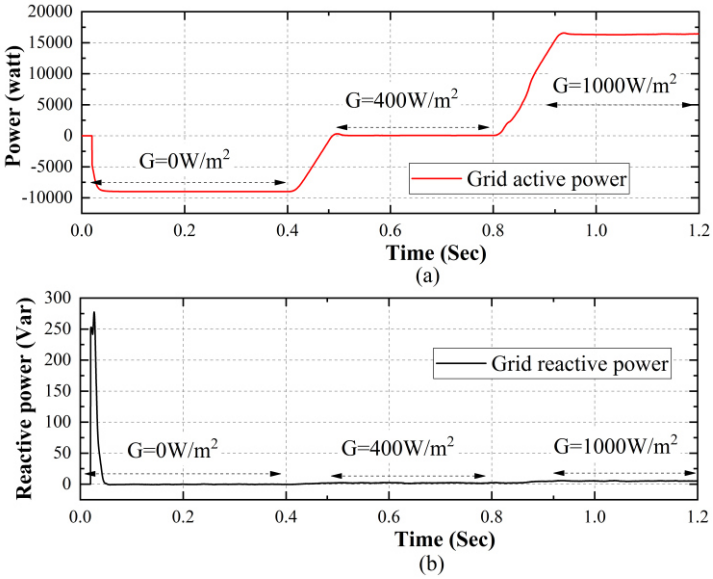

Figure 8. Power profiles of the grid with variation in irradiation level: (a) grid active power plot, (b) grid reactive power plot.

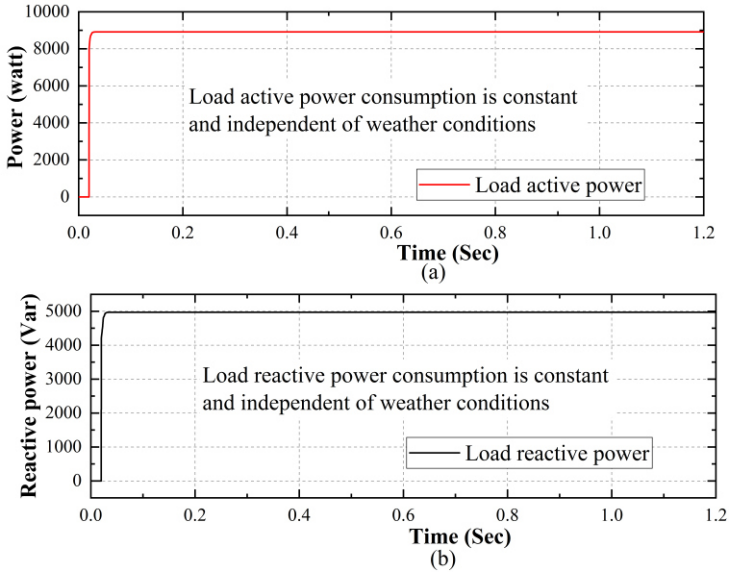

Figure 9. Power profiles of the load with variation in irradiation level: (a) load active power plot, (b) load reactive power plot.

Since the inverter generates 25 kW of active power and the load demand remain constant at 9 kW, the excess (25 kW- 9kW) = 16 W amount of active power is transmitted to the grid. It is observed during this period that the grid starts to receive the excess 16 kW of active power from the PV inverter module as shown in Figure 8(a). Thus, the inverter starts to generate power in excess of the load demand and acts as a source to the grid.

4.2 Analysis of reactive power distribution

In case of reactive power, it is observe that the load reactive power demand remains constant at about 5 kVAR all throughout the three different irradiation levels. This is observed from Figure 9(b). The PV inverter, with the help of the connected capacitor bank, continuous to produce a reactive power in the range of about 5 kVAR irrespective of the irradiation level. Even when the radiation level becomes zero for the first 0.4 sec duration, still the PV inverter continuous to produce this amount of reactive power. This is observed from Figure 7(b). Hence, the total demand of the load in terms of the reactive power is supplied solely by the PV inverter itself. Hence, no reactive power is transferred to the load from the grid as is observed from Figure

8(b). Thus, the total reactive power intake from the grid remains close to zero; thereby, retaining the high power factor of the grid all throughout. This is one of the major advantages of the proposed model where no reactive power is transmitted to the load from the grid and hence, the grid power factor always remains at a high level; although the inverter power factor slightly reduces during the high reactive power demand particularly when the active power demand is on the lower side.

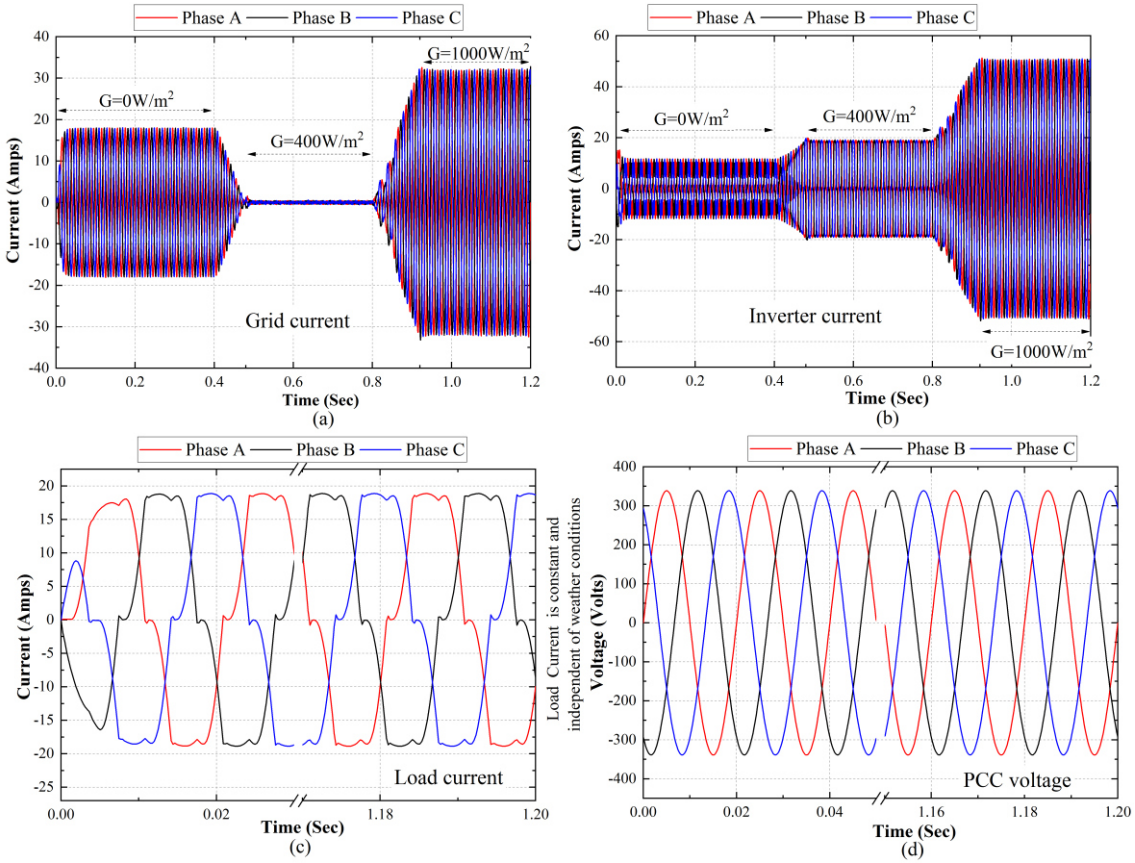

Figure 10. Three phase current profile of the (a) grid, (b) inverter and (c) load; (d) PCC voltage profile.

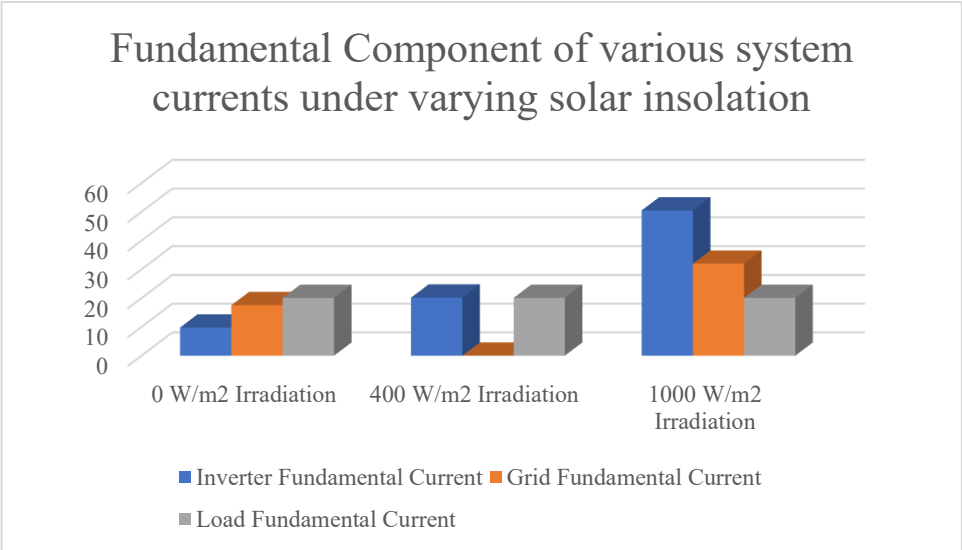

Figure 11. Fundamental component of various system currents under varying irradiation levels.

The current profiles are also shown in Figure 10, where it is easily observed that during the middle period when the radiation level reaches 400 W/m^2, no power is transferred either from the inverter to the grid or vice versa. Thus, the net amount of current transfer remains close to zero. This is clearly observed from Figure 10(a) where we observe that the grid current is remaining close to zero throughout the interval, when the entire active and reactive power is transferred to the load from the inverter only.

4.3 Analysis of reactive power distribution

This method of transferring the total reactive power from inverter to the load end helps in retaining a good power factor of the grid; therefore, minimum harmonic distortion occurs in the grid current. This is observed from the recorded results of Table 3 which separately shows the total harmonic distortion (THD) levels of inverter current, grid current and load current respectively.

Table 3(a). Variation of total harmonic distribution (THD) of the inverter current.

Time duration	Parameter	Fundamental (50 Hz) current (Amps)	THD (%)
t = 0 to 0.4 sec	Inverter current	9.781	29.59
t = 0.4 to 0.8 sec	Inverter current	20.18	14.22
t = 0.8 to 1.2 sec	Inverter current	50.49	5.69

It is observed from Table 3(a) that the THD level reduces, i.e., the power quality improves for the inverter as the irradiation level increases. This is understandable as the irradiation level increases; the active power generation also increases. Since, the reactive power level always remains constant from the inverter, higher contribution of the active power improves the power factor, as well as, reduces the harmonics of the current profile. Figure 12 illustrates graphically the THD of inverter, grid and load currents where we observe that the THD level of grid current always remains well below 2% under all levels of irradiation, which is considered well acceptable as per IEEE standard 519-2014 [23]. This is due to the fact that the reactive power compensation has been provided by the PV inverter it-self and no reactive power is required from the grid. The total amount of reactive power demand of the load has been mitigated by the PV inverter module, even when the irradiation level remains zero. Thus the proposed model serves well to retain good quality of the grid and serve power to the grid as well. The load current THD always remains the same as the load reactive and active power demand remains unaltered throughout.

Table 3(b). Variation of total harmonic distribution (THD) of the grid current.

Time duration	Parameter	Fundamental (50 Hz) current (Amps)	THD (%)
t = 0 to 0.4 sec	Grid current	17.55	1.42
t = 0.4 to 0.8 sec	Grid current	0 (Do not take or supply current from PV+ non-linear load system)	Not applicable
t = 0.8 to 1.2 sec	Grid current	31.98	1.68

Table 3(c). Variation of total harmonic distribution (THD) of the load current.

Time duration	Parameter	Fundamental (50 Hz) current (Amps)	THD (%)
t = 0 to 0.4 sec	Load current	20.09	14.42
t = 0.4 to 0.8 sec	Load current	20.09	14.42
t = 0.8 to 1.2 sec	Load current	20.09	14.42

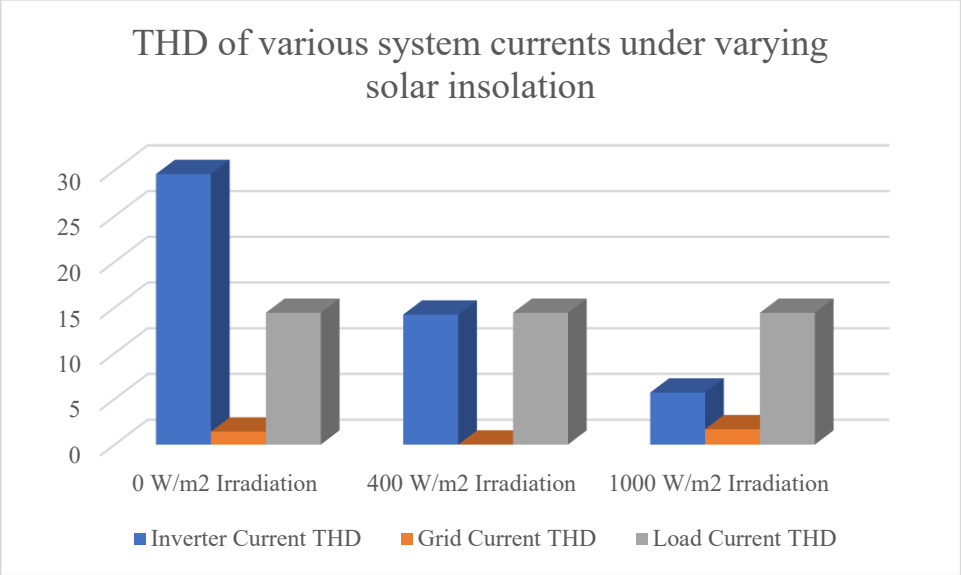

Figure 12. Variation of total harmonic distortion (THD) under varying irradiation levels.

4.4 Comparison of proposed method with contemporary other methods

Table 4. Comparative analysis between proposed method and reference paper [24] & [25].

Feature	Proposed Method	Contemporary Method [25]	Contemporary Method [24]
Grid synchronization	Second-order band-pass filter	Synchronous reference frame PLL	Enhanced-PLL
Connection	Double-stage	Double-stage	Single-stage
Harmonic mitigation	APC method	No special control mechanism	APC method
Reactive power supply	PV inverter	Grid	PV inverter
Power factor (Grid)	Unity	Not specified	Unity
Grid system capacity requirement	No additional requirement	Large enough to fulfil reactive power requirements of non-linear load as well as to retain THD under specified limit.	No additional requirement

The table compares the features of the proposed method with two contemporary methods for grid-tied photovoltaic systems with non-linear loads. The features compared include grid synchronization method, connection type, harmonic mitigation technique, reactive power supply source, power factor at the grid, and grid system capacity requirement. The proposed method utilizes a second-order band-pass filter for grid synchronization, a double-stage connection, APC method for harmonic mitigation, PV inverter for reactive power supply, operates at unity power factor, and requires no additional grid system capacity. In contrast, Contemporary Method [25] uses a synchronous reference frame PLL for grid synchronization, a double-stage connection, no special control mechanism for harmonic mitigation, grid for reactive power supply, not specified power factor, and requires a large grid system capacity. Contemporary Method [24] uses an

Enhanced-PLL for grid synchronization, a single-stage connection, APC method for harmonic mitigation, PV inverter for reactive power supply, operates at unity power factor, and requires no additional grid system capacity.

4.5 Future Scope of work

The proposed method presents a number of opportunities for future research and development, including:

1. Proposal of advanced maximum power point tracking (MPPT) techniques: The proposed method can be further improved by incorporating advanced MPPT techniques that can overcome various weather-related problems, such as partial shading, and improve overall system efficiency.

2. Analysis of grid fault conditions: The proposed method can be tested under various grid fault conditions, including both symmetrical and unsymmetrical faults, to evaluate its performance in maintaining the total harmonic distortion (THD) of the grid current under permissible limits.

3. Integration of low-voltage-ride-through (LVRT) capability: The proposed method can be modified and upgraded to include LVRT functionality, in order to comply with the LVRT requirements of different countries' grid codes. This will guarantee that the system remains linked to the grid at the time of low-voltage events, improving the overall reliability of the system.

These areas of research have the potential to improve the effectiveness and efficacy of the proposed method, and can pave the way for its widespread adoption in the field of renewable energy generation.

5 Conclusion

In this study, we have designed a Double Stage Grid Tied Photovoltaic (DSGTP) model with non-linear load connected, which has the potential to mitigate harmonic problems that arise due to non-linear R-L loads. We used a simplified P&O method to track the maximum power point (MPP), and a PI controller to stabilize the DC link capacitor voltage. Additionally, we used a second-order band-pass filter instead of a PLL for grid synchronization, which reduced the complexity and cost of the system. To mitigate harmonic problems, we used an Active Power Coefficient (APC) control mechanism that ensured that the reactive power demand of the load was always fulfilled by the PV inverter, thereby maintaining the grid current at unity power factor. Through simulations, we demonstrated the successful mitigation of harmonic problems at different weather conditions, and showed that the inverter current waveform remained distorted while the grid current waveform remained sinusoidal throughout the simulation period. Overall, our study provides a valuable contribution to the field of renewable energy generation, demonstrating the potential for effective harmonic mitigation in a DSGTP system with non-linear loads. The graphical representation of the power flow dynamics provides a useful visual aid for understanding the nature of the system during different operating conditions. Further investigations in this field could lead to the progress of more advanced and efficient control mechanisms for renewable energy systems, with potential for widespread adoption in the future.

References

[1] S. B. R. Chowdhury, A. Mukherjee and P. K. Gayen, "Maximum power point tracking of photovoltaic system by Perturb & Observe and Incremental Conductance methods under normal and partial shading conditions," *2021 Innovations in Energy Management and Renewable Resources(52042),* 2021, pp. 1-6, doi: 10.1109/IEMRE52042.2021.9386964.

[2] J. Prasanth Ram, T. Sudhakar Babu, N. Rajasekar, "A comprehensive review on solar PV maximum power point tracking techniques", *Renewable and Sustainable Energy Reviews*, Vol. 67,2017, pp. 826-847, ISSN 1364-0321.

[3] Y. C. Kuo, T. J. Liang, and J. F. Chen, "Novel maximum-powerpoint- tracking controller for photovoltaic energy conversion system", *IEEE transactions on industrial electronics*, vol. 48, no. 3, pp. 594- 601, 2001.

[4] B. Subudhi, and R. Pradhan, "A comparative study on maximum power point tracking techniques for photovoltaic power systems", *IEEE transactions on Sustainable Energy*, vol. 4, no. 1, pp. 89-98, 2012.

[5] M. A. Elgendy, B. Zahawi and D. J. Atkinson, "Assessment of Perturb and Observe MPPT Algorithm Implementation Techniques for PV Pumping Applications," in *IEEE Transactions on Sustainable Energy*, vol. 3, no. 1, pp. 21-33, Jan. 2012, doi: 10.1109/TSTE.2011.2168245.

[6] J. J. Nedumgatt, K. B. Jayakrishnan, S. Umashankar, D. Vijayakumar and D. P. Kothari, "Perturb and observe MPPT algorithm for solar PV systems-modeling and simulation," *2011 Annual IEEE India Conference*, 2011, pp. 1-6, doi: 10.1109/INDCON.2011.6139513.

[7] Chowdhury, S. B. R., Gayen, P. K., Roy, S., & Babu, N. V. (2022). "A Novel MPPT algorithm for PV systems under variable Shading Conditions using Horse Herd Optimization", *Journal of Electrical Systems*, 18(1).

[8] Firat, Y. (2019). "Utility-scale solar photovoltaic hybrid system and performance analysis for eco-friendly electric vehicle charging and sustainable home", *Energy Sources*, Part A: Recovery, Utilization, and Environmental Effects 41 (6):734–45.

[9] Blaabjerg, F., R. Teodorescu, M. Liserre, and A. V. Timbus. (2006). "Overview of control and grid synchronization for distributed power generation systems", *IEEE Transactions on Industrial Electronics* 53 (5):1398–409.

[10] Asiminoael, L., F. Blaabjerg, and S. Hansen. (2007). Detection is key - Harmonic detection methods for active power filter applications. In *IEEE Industry Applications Magazine* 13(4):22–33.

[11] Pragya Gawhade, Amit Ojha,Recent advances in synchronization techniques for grid tied PV system: A review, *Energy Reports*, Volume 7, 2021, Pages 6581-6599, ISSN 2352-4847.

[12] Arulkumar, K., Vijayakumar, D.D., & Palanisamy, K. (2016). Recent advances and control techniques in grid connected PV system - A review. *International Journal of Renewable Energy Research*.

[13] Teodorescu, R, M. Liserre, and P. Rodríguez, "Grid Converters for Photovoltaic and Wind Power Systems," Piscataway, *NJ: IEEE Press/Wiley*, 2011.

[14] M. Karimi-Ghartemani and M. R. Iravani, "A method for synchronization of power electronic converters in polluted and variable-frequency environments," in *IEEE Transactions on Power Systems*, vol. 19, no. 3, pp. 1263-1270, Aug. 2004.

[15] S. Chatterjee and S. Chatterjee, "Simulation of synchronous reference frame PLL based grid connected inverter for photovoltaic application," *2015 1st Conference on Power, Dielectric and Energy Management at NERIST (ICPDEN)*, 2015, pp. 1-6.

[16] M. Mirhosseini, J. Pou and V. G. Agelidis, "Single- and Two-Stage Inverter-Based Grid-Connected Photovoltaic Power Plants With Ride-Through Capability Under Grid Faults," in *IEEE Transactions on Sustainable Energy*, vol. 6, no. 3, pp. 1150-1159, July 2015.

[17] S. Fahad, A. J. Mahdi, W. H. Tang, K. Huang and Y. Liu, "Particle Swarm Optimization Based DC-Link Voltage Control for Two Stage Grid Connected PV Inverter," *2018 International Conference on Power System Technology (POWERCON)*, 2018, pp. 2233-2241.

[18] M. Merai, M. W. Naouar, I. Slama-Belkhodja and E. Monmasson, "An Adaptive PI Controller Design for DC-Link Voltage Control of Single-Phase Grid-Connected Converters," in *IEEE Transactions on Industrial Electronics*, vol. 66, no. 8, pp. 6241-6249, Aug. 2019, doi: 10.1109/TIE.2018.2871796.

[19] H. Afghoul, F. Krim, D. Chikouche and A. Beddar, "Fractional order direct current control algorithm for three-phase grid-connected PV system," *2015 3rd International Conference on Control, Engineering & Information Technology (CEIT)*, 2015, pp. 1-6, doi: 10.1109/CEIT.2015.7233004.

[20] Buchade, P.C., Vyawahare, V.A., & Bhole, V.V. (2014). FractionalOrder control of voltage source inverter (VSI) using Bode's ideal transfer function. *2014 International Conference on Circuits, Systems, Communication and Information Technology Applications (CSCITA)*, 403-407.

[21] M. Cech and M. Schlegel, "The fractional-order PID controller outperforms the classical one," in *Process control 2006*. Pardubice Technical University, 2006, pp.1–6.

[22] A. K. Podder, M. Habibullah and N. K. Roy, "Current THD Analysis of Model Predictive Control based Grid-Connected PV Inverter," *2019 International Conference on Electrical, Computer and Communication Engineering (ECCE), 2019*, pp. 1-6.

[23] "IEEE Recommended Practice and Requirements for Harmonic Control in Electric Power Systems," in *IEEE Std 519-2014 (Revision of IEEE Std 519-1992)*, vol., no., pp.1-29, 11 June 2014, doi: 10.1109/IEEESTD.2014.6826459

[24] A. Kumar , N. Patel , N. Gupta , V. Gupta & B. C. Babu, (2020). Active power coefficient control for grid-tied photovoltaic system under voltage distortions. *Energy Sources*, Part A: Recovery, Utilization, and Environmental Effects, 1-24.

[25] Chowdhury, S. B. R., Maji, A., Gayen, P. K., & Chowdhury, S. K. (2022, November). Performance analysis of PLL based DSGCP (Double Stage Grid Connected Photovoltaic) system with non-linear load under normal and various grid fault conditions. In *2022 IEEE International Conference of Electron Devices Society Kolkata Chapter (EDKCON)* (pp. 29-34). IEEE.